Heliyon 10 (2024) e34556

Contents lists available at ScienceDirect

Heliyon

journal homepage: www.cell.com/heliyon

Research article

# Synthesis, quantum chemical calculations, in silico and in vitro bioactivity of a sulfonamide-Schiff base derivative

Md. Minhazul Abedin [a], Tarun Kumar Pal [a,*], Md. Najem Uddin [b], Mohammad Abdul Alim [c], Md. Chanmiya Sheikh [d], Subrata Paul [a]

[a] Department of Chemistry, Rajshahi University of Engineering & Technology, 6204, Bangladesh
[b] Pharmaceutical Sciences Research Division, BCSIR Laboratories (Dhaka), Bangladesh Council of Scientific and Industrial Research (BCSIR), Bangladesh
[c] Department of Chemistry, Bangabandhu Sheikh Mujibur Rahman Science and Technology University, Gopalganj, 8100, Bangladesh
[d] Department of Chemistry, University of Rajshahi, 6205, Bangladesh

ARTICLE INFO

*Keywords:*
Sulfonamide Schiff base
Experimental and computational methods
Bioavailable drug candidate
Anticancer
Antioxidant

ABSTRACT

The sulfonamide Schiff base compound (E)-4-((4-(dimethylamino)benzylidene)amino)-N-(5-methylisoxazol-3-yl)benzenesulfonamide was successfully prepared and fully characterized. The foremost objective of this study was to explore the molecular geometry of the aforementioned compound and determine its drug likeness characteristics, docking ability as an insulysin inhibitor, anticancer and antioxidant activities. The molecular structure of this compound was optimized using the B3LYP/6−311G+(d,p) level of theory. The compound was completely characterized utilizing both experimental and DFT approaches. Molecular electrostatic potential, frontier molecular orbitals, Fukui function, drug likeness, and in silico molecular docking analyses of this compound were performed. Wave functional properties such as localized orbital locator, electron localization function and non-covalent interactions were also simulated. The compound was screened for anticancer and antioxidant activities using in vitro technique. The observed FT-IR, UV–Vis, and $^1$H NMR results compared with simulated data and both results were fairly consistent. The experimental and computational spectral findings confirm the formation of the Schiff base compound. Both π—π* and n—π* transitions were observed in both experimental and computational UV–Vis spectra. The examined compound followed to Pfizer, Golden Triangle, GSK, and Lipinski's rules. Consequently, it possesses a more favorable absorption, distribution, metabolism, excretion, and toxicity (ADMET) profile, making it a suitable candidate for non-toxic oral drug use. Moreover, the compound exhibited promising insulysin inhibition activity in an in silico molecular docking. The compound showed in vitro anticancer activity against A549 cancer cells with an $IC_{50}$ value of 40.89 μg/mL and moderate antioxidant activity.

## 1. Introduction

Sulfamethoxazole is widely recognized as an antibacterial sulfa drug. One amino group is present in its molecular structure, which participates in the formation of the Schiff base with aromatic aldehyde through a condensation reaction [1,2]. The Schiff base was first designated by the German scientist Hugo Schiff [3]. Schiff base compounds contain more potential azomethine linkage [3,4].

* Corresponding author.
*E-mail addresses:* tkpchem@gmail.com, tkpal@chem.ruet.ac.bd (T.K. Pal).

https://doi.org/10.1016/j.heliyon.2024.e34556
Received 10 February 2024; Received in revised form 11 July 2024; Accepted 11 July 2024

Therefore, they demonstrate a broad spectrum of biological activities. Sulfonamides are also considered potent antimicrobial agents [4]. The sulfonamide Schiff base is produced from a condensation reaction between a sulfa drug (such as sulfamethoxazole, sulfathiazole, etc.) and an aromatic aldehyde [1]. Sulfonamide Schiff bases possess both azomethine and sulfonamide (−$SO_2$–NH−) functional groups. These compounds have been widely used in the medicinal and industrial fields [5,6]. Numerous Schiff bases exhibit a wide range of pharmacological activities, such as antibacterial, antifungal, antimalarial, antiviral, antitumor, antiproliferative, antituberculosis, anticancer, and anti-inflammatory activities [1,7–11]. These compounds have also been used as corrosion inhibitors, catalysts, chemosensors, pigments, thermally stable materials, NLO materials, and powerful chelating agents in the formation of coordination compounds [5,12,13]. Besides, Schiff base compounds including tamoxifen, thiacetazone, and nifuroxazide, are utilized for treating breast cancer, tuberculosis, and intestinal infections, respectively [14,15]. Nowadays, microbial pathogens are a major cause of mortality throughout the world [6,16]. The Corona pandemic is one of the most recent examples of this issue. The primary cause of morbidity and mortality worldwide is the growing resistance of microorganisms to currently available antimicrobial medications [17,18]. Some adverse effects and drug resistance emphasize the importance of discovering new potential drug candidates [17,19]. In computer-aided drug design systems, physicochemical, molecular docking, and ADMET predictions are important criteria for evaluating newly designed compounds. To the best of our knowledge, a comparative study, molecular electrostatic potential (MEP), Fukui function, drug likeness, and topology analyses, as well as anticancer and antioxidant assays of the query molecule have not been published yet. Moreover, computational approaches are increasingly being used to support experimental evidence in the field of chemical analysis today [8,20]. For the above investigations, a sulfonamide Schiff base (E)-4-((4-(dimethylamino)benzylidene)amino)-N-(5-methylisoxazol-3-yl)benzene was synthesized by the condensation method, and its experimental and computational analyses were performed. The geometrical and electronic features of this Schiff base were ascertained experimentally and computationally to ensure the consistency of both results. The spectral analyses including FT-IR, UV–visible, $^1$H NMR and $^{13}$C NMR, were employed to investigate the vibrational behavior, optical characteristics, and molecular geometry. Molecular docking analysis was performed to evaluate the binding capacity of the studied compound with the target proteins. ADMET analysis was performed to determine the drug-likeness characteristics of the compound. Topological and Fukui function analyses were performed to investigate the nature of chemical bonding, electron localization, and reactive sites within the compound. Finally, its anticancer and antioxidant activities were evaluated to determine its medicinal characteristics.

## 2. Experimental approaches

### 2.1. Materials and methods

The starting materials, sulfamethoxazole and 4-(dimethylamino) benzaldehyde, were obtained from Sigma-Aldrich. The solvents were collected from a local chemical supplier. Analytical grade solvents and reactants were used without additional purification. The melting point of the studied compound was determined using the open capillary technique. FT-IR and UV–vis analyses were conducted using SHIMADZU IR Affinity−1S and PG Instruments CT60, respectively, at the Department of Chemistry, Rajshahi University of Engineering & Technology, Bangladesh. The $^1$H NMR (400 MHz) and $^{13}$C NMR (100 MHz) analyses of the final purified compound were performed in DMSO using the JEOL JNM-ECZ400S spectrometer from Okayama University of Science, Japan. The topological parameters were evaluated using Gaussian [21], Multiwfn 3.8 [22], VMD [23], gnuplot, and irfanView. The A549 human non-small-cell lung cancer cell line was acquired from American Type Culture Collection (ATCC, Manassas, VA, USA) and cultured in DMEM medium supplemented with 10 % FBS (Sigma-Aldrich, St. Louis, MO, USA) at the Pharmaceutical Sciences Research Division, BCSIR laboratories (Dhaka), Bangladesh Council of Scientific and Industrial Research (BCSIR), Bangladesh. The cytotoxicity assay used the trypan blue exclusion process, whereas the antioxidant activity assessment used 2,2-diphenyl-1-picrylhydrazyl (DPPH) radical scavenging. The cytotoxicity assay was also conducted at the Pharmaceutical Division, BCSIR laboratories (Dhaka), Bangladesh. In silico molecular docking of the studied compound was performed with two suitable target proteins (PDB ID: 3E4A and PDB ID: 3OFI). ML345 (PubChem-CID: 57390068) was used as a standard compound for docking.

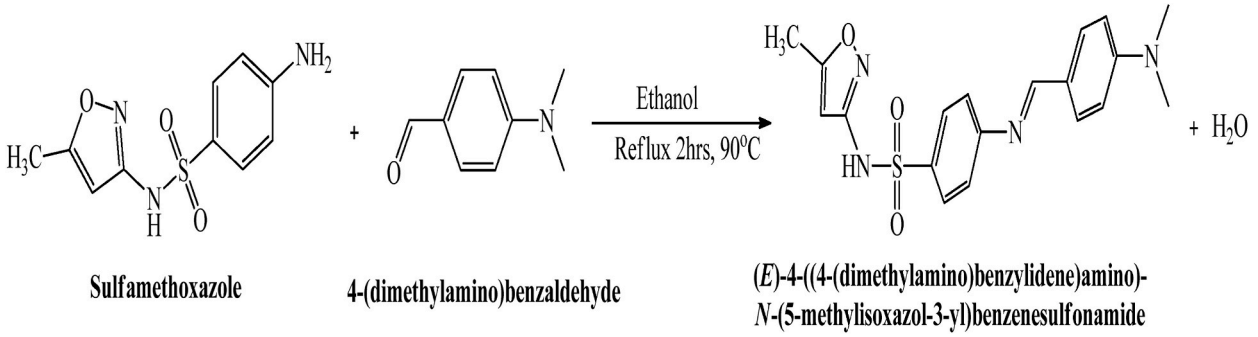


**Scheme 1.** Preparation of the compound.

### 2.2. Preparation of (E)-4-((4-(dimethylamino)benzylidene)amino)-N-(5-methylisoxazol-3-yl)benzenesulfonamide compound

An ethanolic solution of 4-(dimethylamino)benzaldehyde (1.49 g, 0.01 mol) was added to an ethanolic solution of sulfamethoxazole (2.53 g, 0.01 mol). The resulting solution was refluxed for 2 h, yielding light orange colored precipitates (Scheme 1). After filtration, the resulting product was washed with hot ethanol. The light orange colored product was crystallized from the solvent, resulting in a 60 % yield. The melting point of the pure compound was 228 °C.

### 2.3. Computational approach

The DFT method with B3LYP functional and 6−311G+(d,p) basis set was utilized for quantum chemical calculations. Gaussian 09 W and GaussView 6.0.16 packages [24] were used for these calculations. The optimized molecular structure, frontier molecular orbital analysis, molecular electrostatic potential mapping, and theoretical spectral studies were successfully obtained using the Gaussian program.

## 3. Results and discussion

### 3.1. FT-IR spectroscopy analysis

The FT-IR spectrum showed several characteristic absorption bands of the studied compound, as detailed in Table 1. A characteristic band appeared at 1617 $cm^{-1}$, due to azomethine (−HC═N−) group. This band ensures the formation of Schiff base. A stretching band for the secondary amine (N–H) group was found at 3315 $cm^{-1}$ in the spectrum of the compound [4,7,25,26]. The azomethine and secondary amine (N–H) bands appeared at 1634 $cm^{-1}$, and 3446 $cm^{-1}$, respectively in the quantum computational spectrum. The asymmetric and symmetric stretching vibrations of the $SO_2$ group were found at 1345 and 1186 $cm^{-1}$, respectively [26,27], while theoretically these bands were observed at 1334, and 1252 $cm^{-1}$. The C–O group of the sulfamethoxazole portion showed a band at 1250 $cm^{-1}$ [4,7]. The S–N group displayed a band at 940 $cm^{-1}$. Computationally, these bands were found at 1263, and 925 $cm^{-1}$, respectively.

### 3.2. UV–vis spectral analysis

The electronic spectrum of the Schiff base was recorded in the range of 200–800 nm. Electronic transition bands appeared at 225 and 250 nm, which were assigned to the $\pi$—$\pi^*$ transition of the aromatic rings and azomethine group [7,8]. Theoretically, these electronic transition bands were obtained at 288, and 313 nm, respectively. An electronic transition peak was obtained at 278 nm in the spectrum, which can be referred to as $n$—$\pi^*$ electronic transition [8]. Computationally, this band appeared at 362 nm. The key contributions of the HOMO and LUMO transitions in the gas phase were as follows: HOMO to LUMO transition accounted for 96 % at a wavelength of 363 nm (Table 2), H−1 to LUMO contributed 76 % at 313 nm, H−4 to LUMO contributed 18 %, HOMO to L+1 contributed 21 %, and HOMO to L+3 contributed 50 % at a wavelength of 288 nm.

### 3.3. $^1H$ NMR and $^{13}C$ NMR analysis

The $^1H$ NMR and $^{13}C$ NMR findings of the compound are listed in Table 3. In the $^1H$ NMR spectrum of the studied compound, a characteristic peak appeared at 8.40 ppm, which corresponded to the azomethine group [4,7,25–27]. The computational shift of this group was 8.60 ppm. The N−(CH3)2 protons signal appeared in the range of 2.03–3.18 ppm [7,26], whereas computationally, it was found at 2.66–3.56 ppm. The aromatic protons signal was found in the range of 6.15–7.80 ppm [8,26]. A signal at 11.28 ppm was found due to the presence of secondary amine group proton [26]. Computationally, a signal for aromatic protons appeared in the range of 7.20–7.92 ppm and the secondary amine proton signal was not found. Alongside, the experimental spectrum showed signals for the isoxazole and methyl isoxazole protons at 6.09 and 2.19 ppm, respectively [7,8]. These signals were computationally obtained at 7.03 and 2.70 ppm. In the $^{13}C$ NMR spectrum, signals for C1, C2, C3, and C4 were observed at 10.72, 163.50, 120.75, and 155.30 ppm, respectively [7,26]. Theoretically, these signals were appeared at 3.98, 161.40, 83.70, and 145.90 ppm, respectively. Aromatic ring

**Table 1**
Vibrational bands of the studied compound.

| Band | Computational ($cm^{-1}$) | | Experimental ($cm^{-1}$) |
|---|---|---|---|
| | Unscaled | Scaled[a] | |
| υ(N–H) | 3560 | 3446 | 3315 |
| υ(C═N) | 1688 | 1634 | 1617 |
| υ($SO_2$)assym | 1378 | 1334 | 1345 |
| υ($SO_2$)*sym* | 1294 | 1252 | 1186 |
| υ(C–O) | 1305 | 1263 | 1250 |
| υ(S–N) | 956 | 925 | 940 |

[a] scaling factor for B3LYP/6−311G+(d, p) is 0.9679 [28].

**Table 2**
Electronic transitions of the studied compound.

| Computational | | | | | Experimental | |
|---|---|---|---|---|---|---|
| Energy ($cm^{-1}$) | Wavelength (nm) | Osc. Strength | Symmetry | Major contributions | Wavelength (nm) | Transition |
| 27555 | 363 | 1.1003 | Singlet-A | HOMO- > LUMO (96 %) | 278 | $n$—$\pi^*$ |
| 31939 | 313 | 0.0086 | Singlet-A | H-1- > LUMO (76 %) | 250 | $\pi$—$\pi^*$ |
| 34711 | 288 | 0.0221 | Singlet-A | H-4- > LUMO (18 %), HOMO- > L+1 (21 %), HOMO- > L+3 (50 %) | 225 | $\pi$—$\pi^*$ |

**Table 3**
NMR data of query molecule.

| Band | Computational (ppm) | Experimental (ppm) | Band | Computational (ppm) | Experimental (ppm) |
|---|---|---|---|---|---|
| N–H | 8.61 | 11.28 | C1 | 3.98 | 10.72 |
| −HC═N− | 6.72 | 8.40 | C2 | 161.40 | 163.50 |
| Ar–H | 7.20–7.92 | 6.15–7.80 | C3 | 83.70 | 120.75 |
| $N-(CH_3)_2$ | 2.66–3.56 | 2.33–3.18 | C4 | 145.90 | 155.30 |
| Isoxazole | 7.03 | 6.09 | Ar–C | 98.90–146.69 | 96.62–157.69 |
| Isoxazole methyl | 2.70 | 2.19 | CH═N | 147.63 | 191.23 |
| | | | $N(CH_3)$ | 30.76 | 13.12 |

carbons were observed in the range of 96.62–157.69 ppm [26]. Theoretically, these signals were found to be in the range of 98.90–146.69 ppm. Peaks at 191.23, and 13.2 ppm correspond to azomethine and $N(CH_3)_2$ carbons, respectively [7,26]. Computationally, these signals were found at 147.63, and 30.76 ppm, respectively.

### 3.4. Frontier molecular orbitals (FMO) analysis

FMO analysis is used to examine the electronic transition. Optical properties, and chemical reactivity [29,30]. The HOMO and LUMO represent the highest occupied molecular orbital and the lowest unoccupied molecular orbital, respectively [31]. These orbitals participate in chemical reactions, and the reactive zones are governed by the energies of the HOMO and LUMO [26,32,33]. The HOMO orbitals describe electron-donor ability, whereas the LUMO orbitals describe electron-accepting ability [5,34,35]. FMO analysis efficiently delineates the internal charge transfer and reactivity of compounds [36–39]. The reactivity of the sulfonamide Schiff base is higher due to its lower band gap value [12,40,41]. The enhancement of the bioactivity of a compound is governed by a decrease in its electrophilicity index. A significantly lower electrophilicity index value (Table 4) implies that the study compound is highly bioactive and non-toxic [42,43]. The positive and negative regions are represented by red and green colors, respectively [12]. The low softness value (0.27) implies that the molecule under study is very soft and polarizable.

The highest filled orbitals (HOMO) are seen in both the aromatic rings, the bi-substituted amine group, and the azomethine part of the optimized molecule (Fig. 1). While, the LUMO is localized in the benzene rings, azomethine group, nitrogen atom, and $SO_2$ group of the optimized compound.

### 3.5. Molecular electrostatic potential (MEP) analysis

The MEP serves as a pictorial representation of the charge distribution across the molecular surface. It determines the locations of

**Table 4**
Global reactivity factors data of the compound.

| Descriptors | Values |
|---|---|
| HOMO energy | −5.72 |
| LUMO energy | −2.00 |
| Energy gap ($\Delta E_{LUMO\text{-}HUMO}$) | 3.72 |
| Ionization potential (I) | 5.72 |
| Electron affinity (A) | 2.00 |
| Chemical hardness (η) | 1.86 |
| Chemical softness (S) ($eV^{-1}$) | 0.27 |
| Chemical potential (μ) | −3.86 |
| Electronegativity (χ) | 3.86 |
| Electrophilicity index (ω) | 4.01 |
| Electro-donating power ($\omega^-$) | 6.17 |
| Electro-accepting power ($\omega^+$) | 2.31 |
| Net electrophilicity ($\Delta\omega^{\pm}$) | 8.48 |
| Maximum charge transfer index ($\Delta N_{max.}$) | 2.08 |

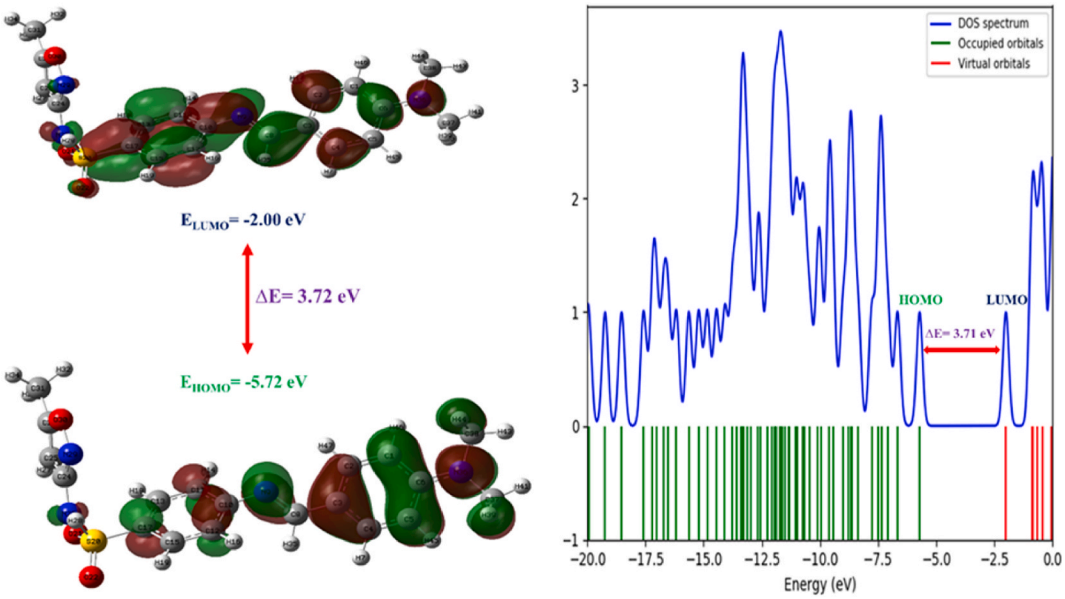


**Fig. 1.** Depiction of the HOMO, LUMO energies, and DOS spectrum.

electrophilic, nucleophilic, and neutral sites which are visually depicted through a color code [35]. The spatial arrangement of molecular electrostatic potentials is analogous to the chemical reactivity and formation of intense bonds at specific active sites [37,44]. MEPs are intricately linked to the chemical properties, electronegativity, and dipole moment [37]. The blue region corresponds to a positive-charge center (a nucleophilic zone), while the red region corresponds to a negative-charge density (an electrophilic zone). Neutral electrostatic zones are denoted by the color green [45]. The Schiff base showed the most negative zones on the oxygen atoms (O21, O22, O30) of the sulfamethoxazole portion and the nitrogen atom (N9) of the azomethine group (Fig. 2), making them attractive sites for electrophilic attack. Positive zones are located around the hydrogen atoms of the amino group (H28), the hydrogen atoms (H39, H40, H41, H42, H43, H44) of the methyl groups, and the sulfur atom (S20) of the $SO_2$ group, representing preferential nucleophilic interaction sites [35].

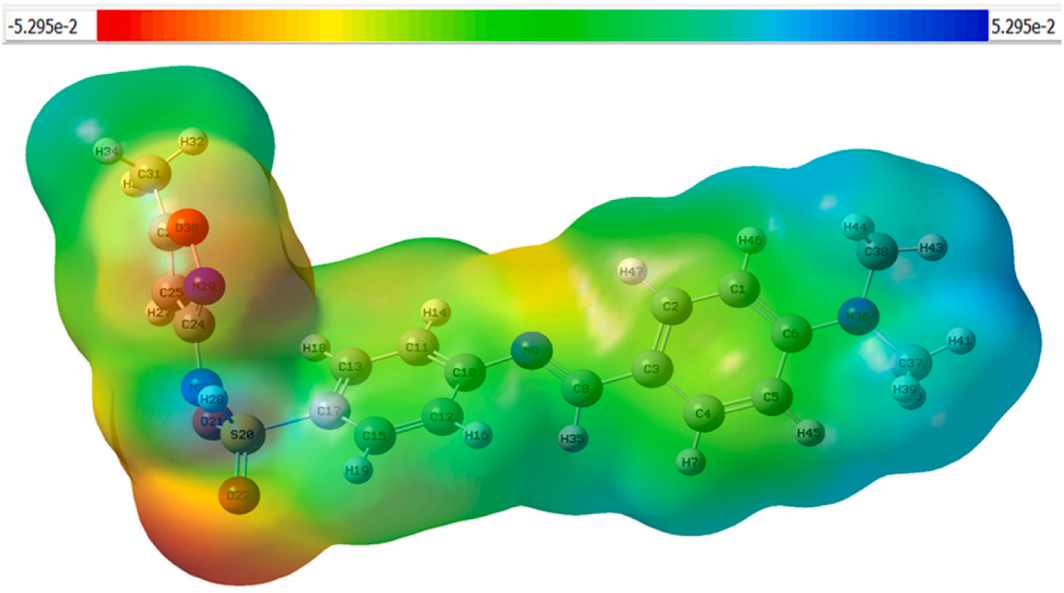


**Fig. 2.** Pictorial view of the MEP surface.

### 3.6. Electron localization function/localized orbital locator studies

The topological assessment of the studied compound was achieved by determining two emerging factors: ELF and LOL, facilitated by the Multiwfn 3.8 command-line software [22]. LOL's chemical composition is identical to that of ELF, because both components are determined by the kinetic energy density [46]. The extent of electron-cloud confinement within a certain atomic/molecular zone is effectively governed by Pauli expulsion, which determines the magnitude of ELF [47,48]. Various color bands, including red (high), green (mid), and blue (low) indicate the extent of electron confinement in the ELF and LOL graphical plots, as visualized in Fig. 3 (a) and (b). The ELF and LOL plots reveal that areas proximate to C4, C5, C6, C37, C38, O22, and N36 have lower values, as represented by the rounded blue band (depletion zones). In contrast, areas around the H7, H41, H43, and H45 atoms (Fig. 3 (a)) have higher values, denoted by the rounded red bands (localized or confined zones), which consist of localized bonded, non-bonded, or lone pairs [49]. Similarly, the LOL orbital localization parameter shows that the annular red color palette indicates greater orbital localization, whereas the blue circles denote lower localization levels (Fig. 3 (b)).

### 3.7. NCI-RDG index analysis

The reduced density gradient (RDG) is a valuable tool for analyzing various weak interactions in a molecule. The RDG-based NCI isosurfaces were generated using Multiwfn 3.6 and VMD 1.9.3 software, which provide the positions and nature of noncovalent interactions in the compound [50,51]. The gradient plot of RDG versus electron density is depicted in Fig. 4. This plot indicates the strength of various interactions in a molecule. These interactions influence the binding mode between the ligand and protein [52,53]. A value approximately equal to zero (sign($\lambda_2$)$\rho \approx 0$) indicates weak van der Waals forces, while negative (sign($\lambda_2$)$\rho < 0$) and positive

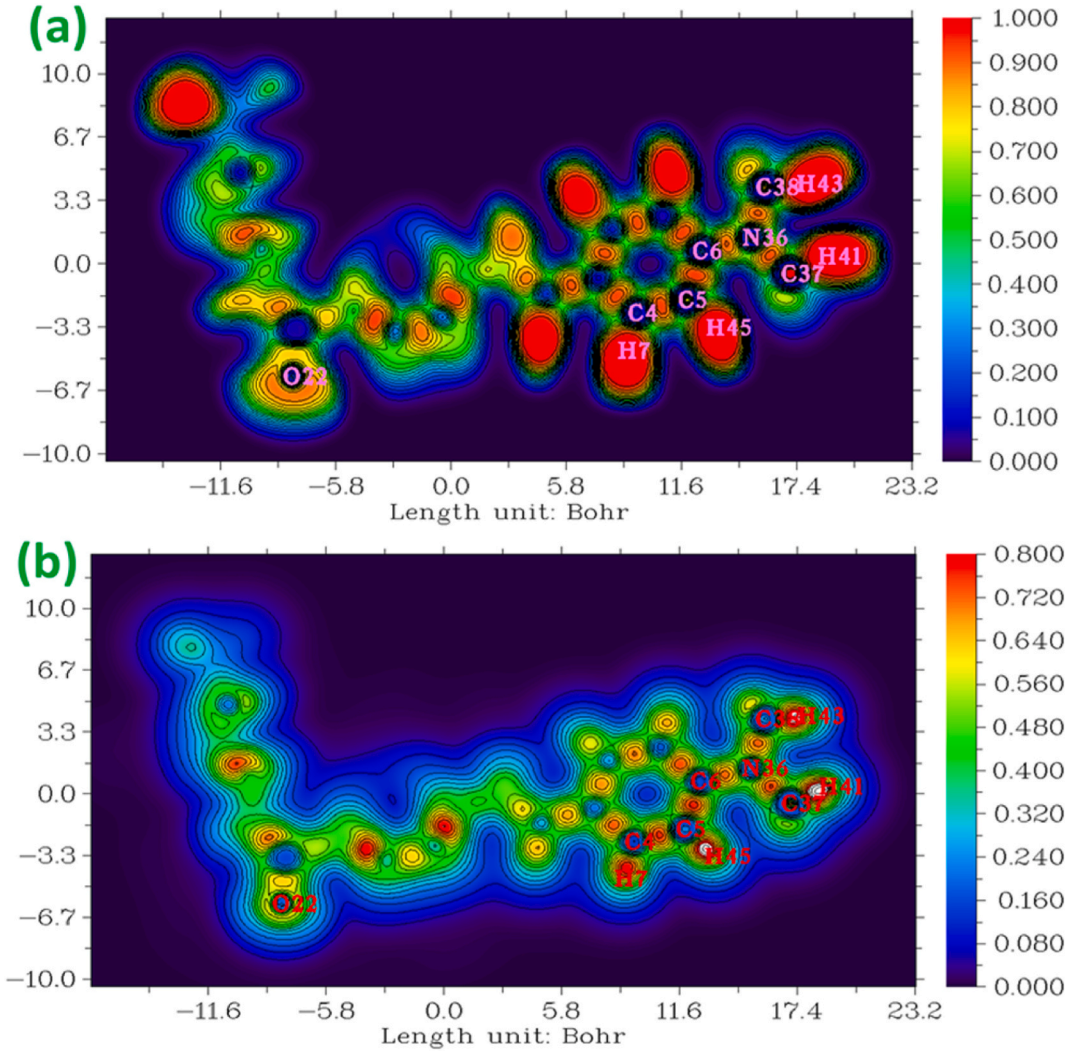


**Fig. 3.** (a) Electron localization function (ELF) map and (b) Localized orbital locator (LOL) map of the studied compound in the gas

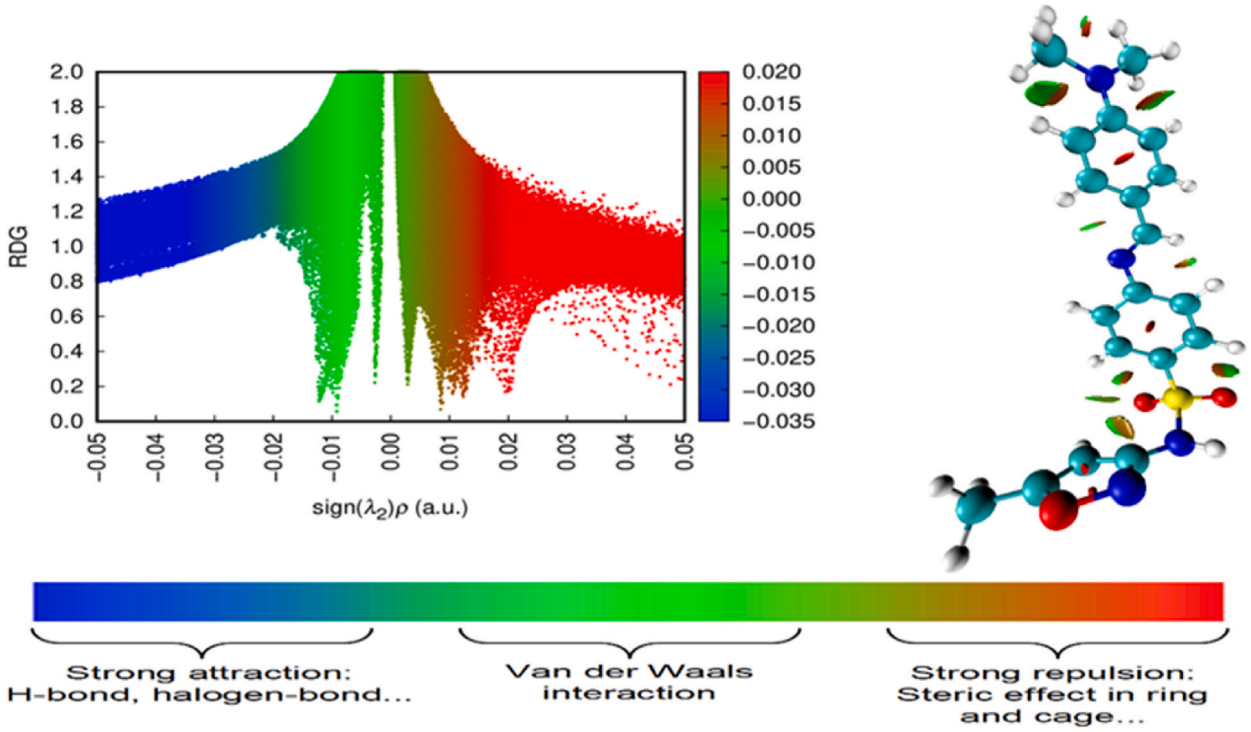


**Fig. 4.** RDG plot for the synthesized compound.

(sign($\lambda_2$)$\rho > 0$) values demonstrate strong attractive (H-bonding) and repulsive (steric effects) forces, respectively [54]. In Fig. 4, the red color on the ring system indicates a steric effect, while the green color is due to van der Waals (vdW) interactions, resulting in low electron density at this position.

### 3.8. Fukui function study

The Fukui function in quantum computation gives quantitative information about the electrophilicity or nucleophilicity of each atom. It relies on Mulliken population inspection [55]. A molecular structure's reactive sites is determined by its local softness and Fukui function. Atomic charges were used to assess Fukui functions by analyzing Mulliken's population [55,56]. In order to compute the Fukui function, the below formulas are employed:

$f^{+}(r) = q_r\ (N+1) - q_r\ (N)$ (for nucleophilic attack)

$f^{-}(r) = q_r\ (N) - q_r\ (N-1)$ (for electrophilic attack)

$f^{0}\ (r) = (q_r\ (N+1) - q_r\ (N-1)/2$ (for radical attack)

In these formulas, $q_r$ is the atomic charge at the rth atomic site in the neutral (N), anionic (N+1), and cationic (N−1) chemical species. One of the topical characteristics is softness, which is used in the Fukui analysis [57]. The local softness can be represented as follows: $S^{+}{}_r f^{+}{}_r = f^{+}{}_r S$ for nucleophilic attack, $S_r^{-} f^{+}{}_r = f_r^{-} S$ for electrophilic attack and $S_r^0 f_r^0 = f_r^0 S$ for radical attack. Here +, -, and 0 signs denote nucleophilic, electrophilic, and radical attack, respectively. The Fukui functions, dual descriptors, softness, and Mulliken charges for each atom of the studied compound are listed in Table 5. It is found that atom 23 N is more electrophilic in attack because it has a larger negative dual descriptor value of −0.692. While, 25C is more nucleophilic in attack because it has a larger positive dual descriptor value of 0.695. The electrophilic sites [($\Delta f_r$<0)] of the studied molecule are 30O, 31C, 2C, 11C, 17C, 12C, 6C, 10C, 15C, 13C, S20, 8C, 38C, 26C, and 23 N. The nucleophilic sites [($\Delta f_r$ >0)] of the studied molecule are 4C, 9 N, 24C, 36 N, 22O, 1C, 5C, 3C, 37C, 27H, O21, and 25C. The behavior of a molecule in electrophilic and nucleophilic attacks during a reaction depends on its local properties. In the studied compound, electrophilic attack is favored over nucleophilic and radical attacks.

### 3.9. Drug likeness and ADMET analysis

Assessment of ADMET (absorption, distribution, metabolism, excretion, and toxicity) for newly investigated molecules is a vital aspect of discovering and developing new medications. At a therapeutic dose, a medication candidate should exhibit appropriate ADMET properties and sufficient efficacy against the therapeutic target [58–60]. Recently, many in silico models have been developed

**Table 5**
Fukui function parameters of the Schiff base compound.

| Atom | Mulliken atomic charges | | | Fukui functions | | | Dual des. | Local softness | | |
|---|---|---|---|---|---|---|---|---|---|---|
| | 0, 1 (N) | N +1 (−1, 2) | N−1 (1,2) | $f_r^+$ | $f_r^-$ | $f_r^0$ | $\Delta f_r$ | $S_r^+ f_r^+$ | $S_r^- f_r^-$ | $S_r^0 f_r^0$ |
| 1C | −0.028 | 0.036 | −0.069 | 0.064 | 0.041 | 0.053 | 0.023 | 0.014 | 0.009 | 0.011 |
| 2C | 0.017 | 0.063 | −0.036 | 0.046 | 0.053 | 0.050 | −0.008 | 0.010 | 0.012 | 0.011 |
| 3C | −0.034 | 0.023 | −0.045 | 0.057 | 0.011 | 0.034 | 0.047 | 0.012 | 0.002 | 0.007 |
| 4C | 0.009 | 0.061 | −0.041 | 0.052 | 0.050 | 0.051 | 0.002 | 0.011 | 0.011 | 0.011 |
| 5C | −0.035 | 0.037 | −0.077 | 0.072 | 0.042 | 0.057 | 0.030 | 0.016 | 0.009 | 0.012 |
| 6C | 0.056 | 0.084 | 0.011 | 0.028 | 0.045 | 0.037 | −0.017 | 0.006 | 0.010 | 0.008 |
| 7H | 0.000 | 0.000 | 0.000 | 0.000 | 0.000 | 0.000 | 0.000 | 0.000 | 0.000 | 0.000 |
| 8C | 0.089 | 0.122 | −0.032 | 0.033 | 0.121 | 0.077 | −0.088 | 0.007 | 0.026 | 0.017 |
| 9 N | −0.147 | −0.093 | −0.199 | 0.054 | 0.052 | 0.053 | 0.002 | 0.012 | 0.011 | 0.012 |
| 10C | 0.052 | 0.062 | 0.019 | 0.010 | 0.033 | 0.022 | −0.023 | 0.002 | 0.007 | 0.005 |
| 11C | 0.008 | 0.047 | −0.043 | 0.039 | 0.051 | 0.045 | −0.012 | 0.009 | 0.011 | 0.010 |
| 12C | −0.001 | 0.030 | −0.047 | 0.031 | 0.046 | 0.039 | −0.015 | 0.007 | 0.010 | 0.008 |
| 13C | 0.028 | 0.056 | −0.028 | 0.028 | 0.056 | 0.042 | −0.028 | 0.006 | 0.012 | 0.009 |
| 14H | 0.000 | 0.000 | 0.000 | 0.000 | 0.000 | 0.000 | 0.000 | 0.000 | 0.000 | 0.000 |
| 15C | 0.030 | 0.061 | −0.025 | 0.031 | 0.055 | 0.043 | −0.024 | 0.007 | 0.012 | 0.009 |
| 16H | 0.000 | 0.000 | 0.000 | 0.000 | 0.000 | 0.000 | 0.000 | 0.000 | 0.000 | 0.000 |
| 17C | −0.036 | −0.004 | −0.080 | 0.032 | 0.044 | 0.038 | −0.012 | 0.007 | 0.010 | 0.008 |
| 18H | 0.000 | 0.000 | 0.000 | 0.000 | 0.000 | 0.000 | 0.000 | 0.000 | 0.000 | 0.000 |
| 19H | 0.000 | 0.000 | 0.000 | 0.000 | 0.000 | 0.000 | 0.000 | 0.000 | 0.000 | 0.000 |
| 20S | 0.462 | 0.462 | 0.430 | 0.000 | 0.032 | 0.016 | −0.031 | 0.000 | 0.007 | 0.003 |
| 21O | −0.312 | 0.462 | 0.430 | 0.774 | −0.742 | 0.016 | 0.515 | 0.169 | −0.162 | 0.003 |
| 22O | −0.321 | −0.287 | −0.338 | 0.034 | 0.017 | 0.026 | 0.017 | 0.007 | 0.004 | 0.006 |
| 23 N | 0.024 | −0.295 | −0.349 | −0.32 | 0.3729 | 0.02695 | −0.692 | −0.0695 | 0.08129 | 0.00588 |
| 24C | 0.024 | 0.05 | 0.002 | 0.026 | 0.022 | 0.024 | 0.004 | 0.00567 | 0.0048 | 0.00523 |
| 25C | 0.076 | 0.077 | 0.77 | 0.001 | −0.694 | −0.3465 | 0.695 | 0.00022 | −0.1513 | −0.0755 |
| 26C | −0.037 | −0.028 | −0.4 | 0.009 | 0.363 | 0.186 | −0.354 | 0.00196 | 0.07913 | 0.04055 |
| 27H | −0.083 | 0.093 | 0.0729 | 0.176 | −0.156 | 0.01005 | 0.3319 | 0.03837 | −0.034 | 0.00219 |
| 28H | 0 | 0 | 0 | 0 | 0 | 0 | 0 | 0 | 0 | 0 |
| 29 N | 0 | 0 | 0 | 0 | 0 | 0 | 0 | 0 | 0 | 0 |
| 30O | −0.134 | −0.123 | −0.146 | 0.011 | 0.012 | 0.0115 | −0.001 | 0.0024 | 0.00262 | 0.00251 |
| 31C | −0.068 | −0.055 | −0.083 | 0.013 | 0.015 | 0.014 | −0.002 | 0.00283 | 0.00327 | 0.00305 |
| 36 N | 0.07 | 0.099 | 0.055 | 0.029 | 0.015 | 0.022 | 0.014 | 0.00632 | 0.00327 | 0.0048 |
| 37C | 0.002 | 0.032 | 0.0423 | 0.03 | −0.040 | −0.0052 | 0.0703 | 0.00654 | −0.0088 | −0.0011 |
| 38C | −0.003 | −0.123 | −0.023 | −0.12 | 0.0204 | −0.0498 | −0.1404 | −0.0262 | 0.00445 | −0.0109 |

to predict the ADMET properties of the newly synthesized compound. In this study, the web tool ADMETlab 2.0 [59]was used to calculate the ADMET properties of the studied compound. Lipinski's rule suggests that a compound must possess a number of hydrogen bond donors (nHBD) $\leq$ 5, hydrogen bond acceptors (nHBA) $\leq$ 10, molecular weight (MW) $\leq$500, octanol/water partition coefficient (logP) $\leq$5, to act as an orally consumed bioavailable drug [61,62]. The discussed compound pursued all the conditions without any violations (Table 6). Therefore, it can be considered a bioavailable oral drug. The Pfizer rule indicates toxicity hazards. The findings reveal that the compound is nontoxic as a drug candidate. The GSK rule and Golden Triangle rule are other rules of thumb for describing the favorability of the ADMET profile of molecules. The statements of the rules are MW $\leq$ 400 with logP $\leq$4, and 200 $\leq$ MW $\leq$ 500; −2 $\leq$ logD $\leq$5 for the GSK rule and the Golden Triangle rule, respectively. The compound strongly follows both rules and possesses a favorable ADMET profile (Table 6). The absorption profile of the compound was determined by visualizing its properties, including Caco-2 permeability, MDCK permeability, Pgp-inhibitor, Pgp-substrate, HIA, F20 %, and F30 %. All the absorption profile indicators lie within the acceptable limits. Therefore, the compound has good intestinal absorptivity, oral bioavailability, and uptake efficiency. The volume distribution (VD) value reveals that the compound can easily bind to plasma proteins and distribute in the body

**Table 6**
ADMET prediction values of the studied compound.

| Parameter | Observed value | Parameter | Observed value | Parameter | Observed value |
|---|---|---|---|---|---|
| Hydrogen Bond Donor | 1 | Pgp-substrate | 0.004 | Rat Oral Acute Toxicity | 0.088 |
| Hydrogen Bond Acceptor | 7 | Pgp-inhibitor | 0.205 | FDAMDD | 0.439 |
| Molecular Mass | 384.13 | Caco2 permeability | −4.614 | AMES Toxicity | 0.354 |
| Polar Surface Area | 87.8 | MDCK permeability | 1.5e-05 | H-HT | 0.581 |
| Water solubility | −4.526 | HIA | 0.005 | Respiratory Toxicity | 0.104 |
| Rotatable Bonds | 6 | $F_{20\ \%}$ | 0.002 | Eye Corrosion | 0.003 |
| LogP | 3.948 | $F_{30\ \%}$ | 0.002 | Eye Irritation | 0.036 |
| Skin Sensitization | 0.223 | Golden Triangle | Accepted | hERG Blockers | 0.1 |
| SAscrore | 2.391 | Lipinski Rule | Accepted | $IGC_{50}$ | 4.49 |
| BBB permeability | 0.465 | Pfizer Rule | Accepted | $LC_{50}FM$ | 5.026 |
| VDss (human) | 0.516 | GSK Rule | Accepted | $LC_{50}DM$ | 5.01 |

fluid. The blood–brain barrier (BBB) penetration value indicates that the compound can act in the central nervous system (CNS). In addition, this compound has no hERG (ether-a-go-go gene) inhibition activity. Obtaining a lower synthetic accessibility score (SAscore) indicates that the preparation of this drug-like compound will be very easy. The toxicity-measurement parameters, hERG blockers, rat oral acute toxicity (ROAT), skin sensitization (SS), eye corrosion/irritation (EC/EI), and respiratory toxicity (RT) as well as all the above mentioned parameters indicate that the studied compound may be safe as a drug component.

### 3.10. *In silico molecular docking analysis*

The molecular docking study is mainly utilized for determining the binding pattern of a molecule (ligand) to a target protein. The findings inform about the investigated compound, which may or may not be used as drug component in future [63,64]. Pass online (https://www.way2drug.com/PassOnline/index.php) is a versatile and reliable web tool for easily predicting the biological activity profile of the query molecule [43]. The web tool suggests that the synthesized molecule is a good inhibitor of insulysin, with a $P_a$ (probability to be active) value of 0.950. Two suitable and previously studied target proteins (PDB ID: 3E4A and PDB ID: 3OFI) were chosen based on docking studies of the studied compound and downloaded in the.pdb format from the RCSB Protein Data Bank (https://www.rcsb.org/structure) web server [61,62]. The crystal structures of the human insulin-degrading enzyme (PDB ID: 3E4A and PDB ID: 3OFI) were collected, and polar hydrogens were inserted after eliminating heteroatoms [65,66]. The grid was spaced 0.375 Å apart, with a grid dimension of 40 × 40 × 40 Å for both targets. The centers were located at x = −95.274, y = 65.332, and z = 3.496 for 3E4A and x = 95.409, y = −65.459, and z = 18.382 for 3OFI, respectively. The software programs used in the docking study were AutoDockTools-1.5.6, Autodock_vina_1_1_2, PyMOL-2.5.7 graphics tool, and LigPlot + v.2.2.8 [67]. The binding pattern of compound−3E4A reveals that the two oxygen atoms of –$SO_2$- bind to the amino acids Ser132 and Arg892 (Fig. 5(a)), the nitrogen atom of sulfonamide binds to Ser816, and the nitrogen atom of azomethine binds to the Ser128 amino acid via hydrogen bonding interactions, with bond distances of 2.81, 3.31, 3.19, and 3.15 Å, respectively. The carbon and hydrogen atoms of the rings in the compound bind to the amino acids Glu817, Glu182, Gln11, His112, Arg824, Phe815, Phe820, and Ser137 via hydrophobic interactions. In contrast, the binding pattern of compound–3OFI revealed that the amino acids Ser132 and Arg892 bind to the oxygen atoms of the sulfonamide group, while the nitrogen atom of the sulfonamide binds to Ser816 through hydrogen bonding interactions (Fig. 5(b)), with bond distances of 2.81, 3.04, and 3.04 Å, respectively. The carbon and hydrogen atoms, along with the oxygen atoms of the sulfamethoxazole portion and the nitrogen atom of the azomethine group, bind to the amino acids Glu817, Phe115, Phe820, Arg824, His112, Glu182, Glu111, and Ser137 via hydrophobic interactions. The compound ML345 (PubChem-CID: 57390068) was used as a reference for comparison with the studied compound. The binding modes of the reference compound (ML345) with 3E4A and 3OFI were visualized in Fig. 6(a) and (b). The binding affinities resulting from the interaction of ML345 with the two target proteins were −8.3 kcal/mol for 3E4A and −8.9 kcal/mol for 3OFI, respectively, whereas the binding affinities for the discussed compound's

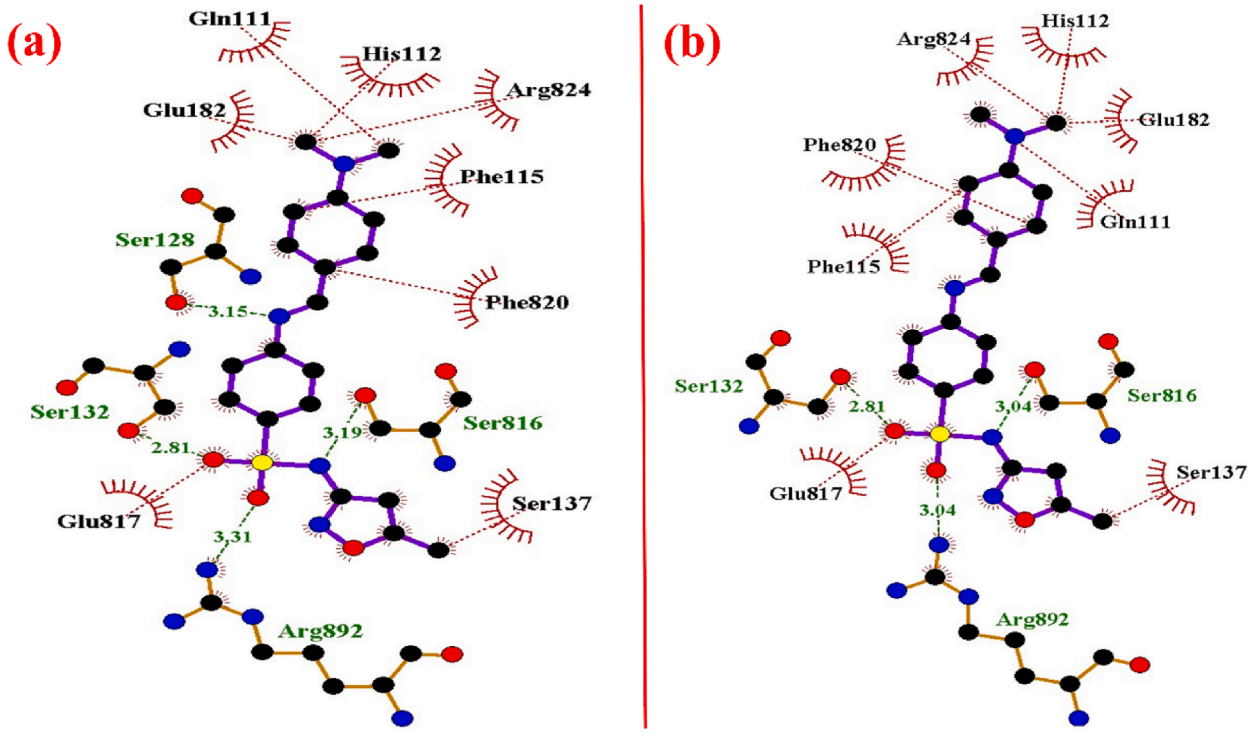


**Fig. 5.** Binding pattern of the compound with (a) 3E4A and (b) 3OFI.

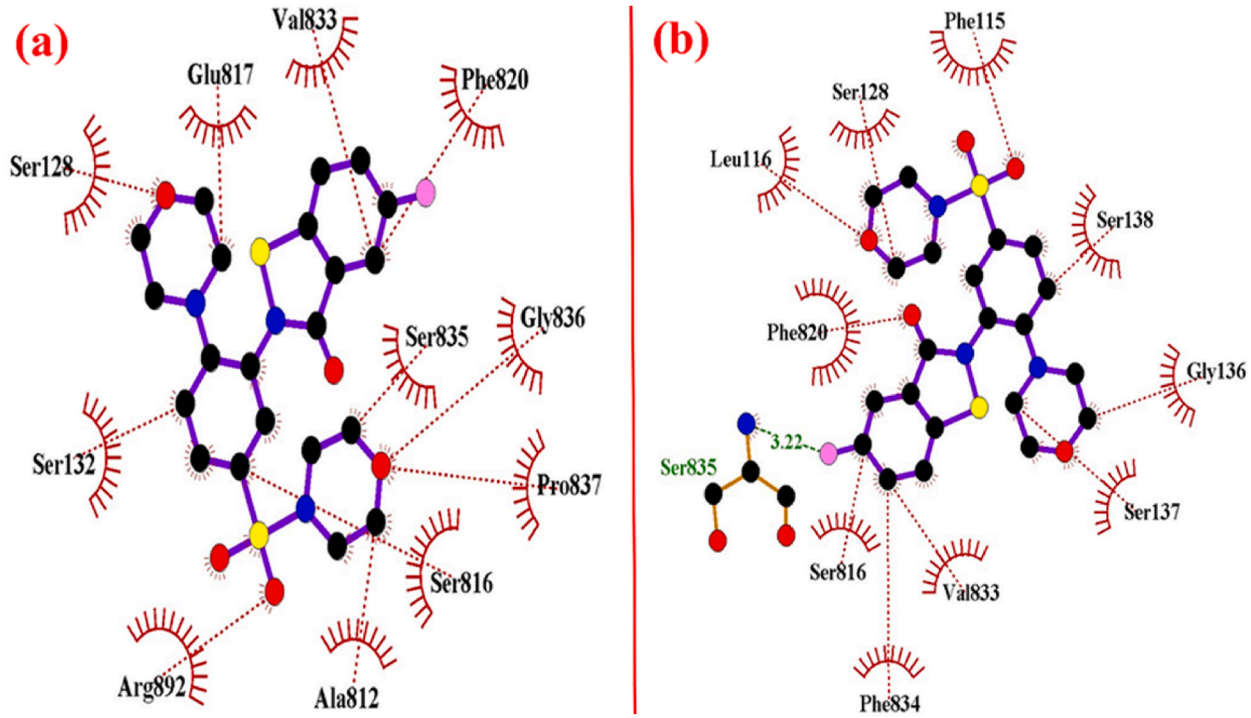


**Fig. 6.** Binding pattern of ML345 with (a) 3E4A and (b) 3OFI.

interaction with the two target proteins were found to be −9.0 and −8.8 kcal/mol, respectively. The results reveal that the studied compound exhibits potent insulysin inhibition activity compared with the reference compound, ML345.

### *3.11. Antioxidant activity analysis*

Species with one or more unpaired electrons are known as free radicals. Antioxidants are reciprocal to free radicals that act as inhibitors of free radical chain reactions. The detrimental effects of free radicals are not limited to foodstuffs, they are also responsible for many diseases in the human body, such as autoimmune disorders, Parkinson's disease, neurological diseases, cancer, pulmonary diseases, aging, cataracts, rheumatoid arthritis, cardiovascular diseases, and Alzheimer's disease [68–76]. The antioxidant activity of the synthesized Schiff base was assessed using the established DPPH method. The very stable free radical 2,2-diphenyl-1-picrylhydrazyl (DPPH) is highly reactive towards other free radicals and scavenges them. The free radical scavenging activity of the studied compound at different concentrations was measured using a UV–visible spectrophotometer at a wavelength of 517 nm [77]. A primary antioxidant, butylated hydroxy toluene (BHT), was used as the reference antioxidant in this study (Fig. 7). The LC50 value for the studied compound was 7.90 ppm, whereas that of BHT was 5.12 ppm. In comparison with the $LC_{50}$ value of BHT, the studied compound exhibited moderate antioxidant activity.

### *3.12. In vitro anticancer activity analysis*

In vitro anticancer activity analysis of the studied compound was conducted using lung cancer A549 cells as the experimental model. The resulting $IC_{50}$ value after 48 h of incubation was found to be 40.89 μg/mL. The effect of the compound on cell viability is depicted by the concentration versus cell viability curve shown in Fig. 8, which indicates a decrease in cell viability with increasing concentration. A negative control consisting of 1 % DMSO was included to assess the anticancer activity.

Cell morphology and viability, indicating the presence of live and dead cells. These cells were visualized using the trypan blue dye exclusion process. In this process, live cells do not bind to the dye, whereas dead cells do. To account for the dead cells in the matrix, a sophisticated cell counting device (LUNA-II™, Analytikjena, South Korea) was used. Images of the cancer cell matrix containing dead cells (Fig. 9(a–d)) after incorporation of the studied compound were captured using an inverted microscope.

## 4. Conclusion

In this study, a sulfonamide Schiff base compound (E)-4-((4-(dimethylamino)benzylidene)amino)-N-(5-methylisoxazol-3-yl)benzene was effectively synthesized. This compound was completely characterized using spectroscopic approaches (like FT-IR, UV–Vis, and $^1$H NMR spectroscopy) and DFT approaches. The experimental results were compared to the simulation data. Both data agreed

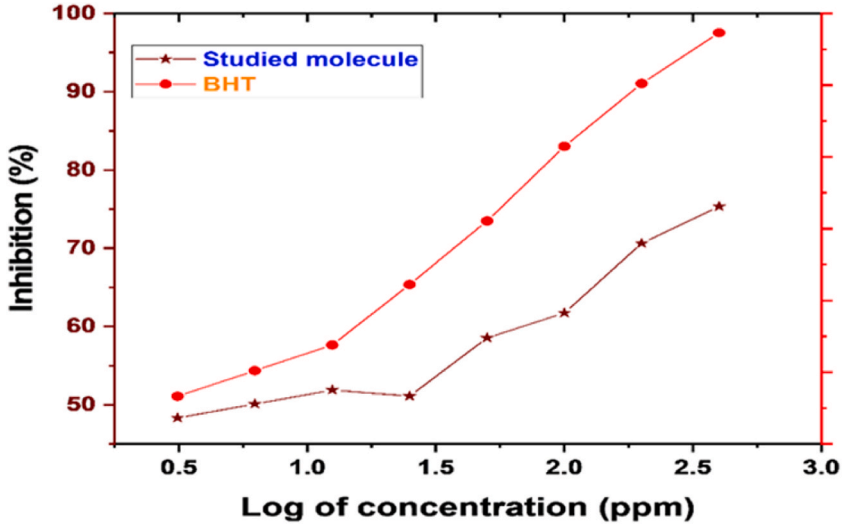


**Fig. 7.** Free radical scavenging activity graph for the substances.

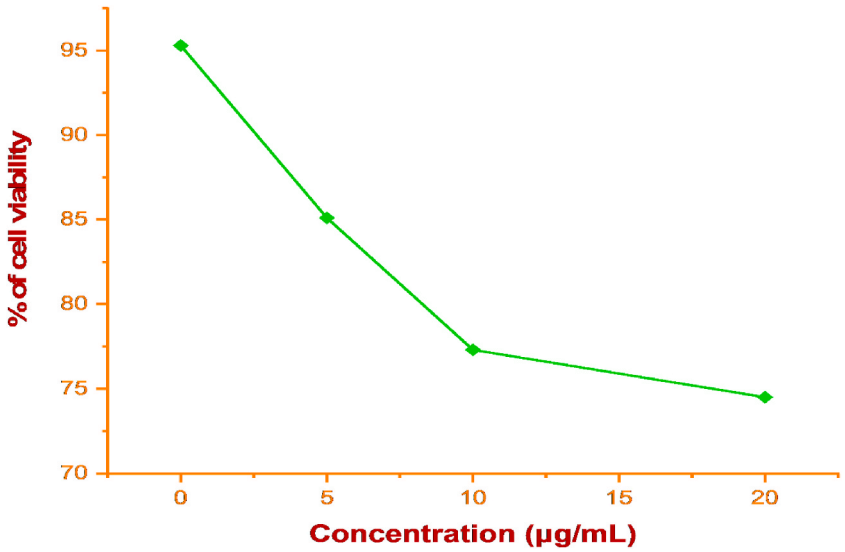


**Fig. 8.** Plot for anticancer activity of the compound after 48 h incubation.

well with each other. The azomethine group showed a characteristic band at 1617 $cm^{-1}$ in FT-IR and a peak at 8.40 ppm in $^{1}H$ NMR spectra. The studied compound exhibited higher reactivity with a lower band gap. The studied compound followed Lipinski's rule, the Pfizer rule, the Golden Triangle, the GSK rule, as well as other ADMET properties, and it can be used as an orally bioavailable drug candidate. The docking results indicated that the compound exhibited good insulysin inhibition activity. In addition, this compound exhibited considerable antioxidant activity. The $IC_{50}$ value of this compound was 40.89 µg/mL. There are no data on its biological application (such as antibacterial, antiviral, antifungal, anti-inflammatory, etc.), corrosion inhibition activity, or metal complexes, which can be investigated in the future.

## Data availability statement

Data will be made available from the corresponding author upon reasonable request.

## CRediT authorship contribution statement

**Md. Minhazul Abedin:** Writing – original draft, Visualization, Formal analysis, Data curation, Conceptualization. **Tarun Kumar Pal:** Writing – review & editing, Supervision, Software, Methodology, Investigation, Conceptualization. **Md. Najem Uddin:** Formal

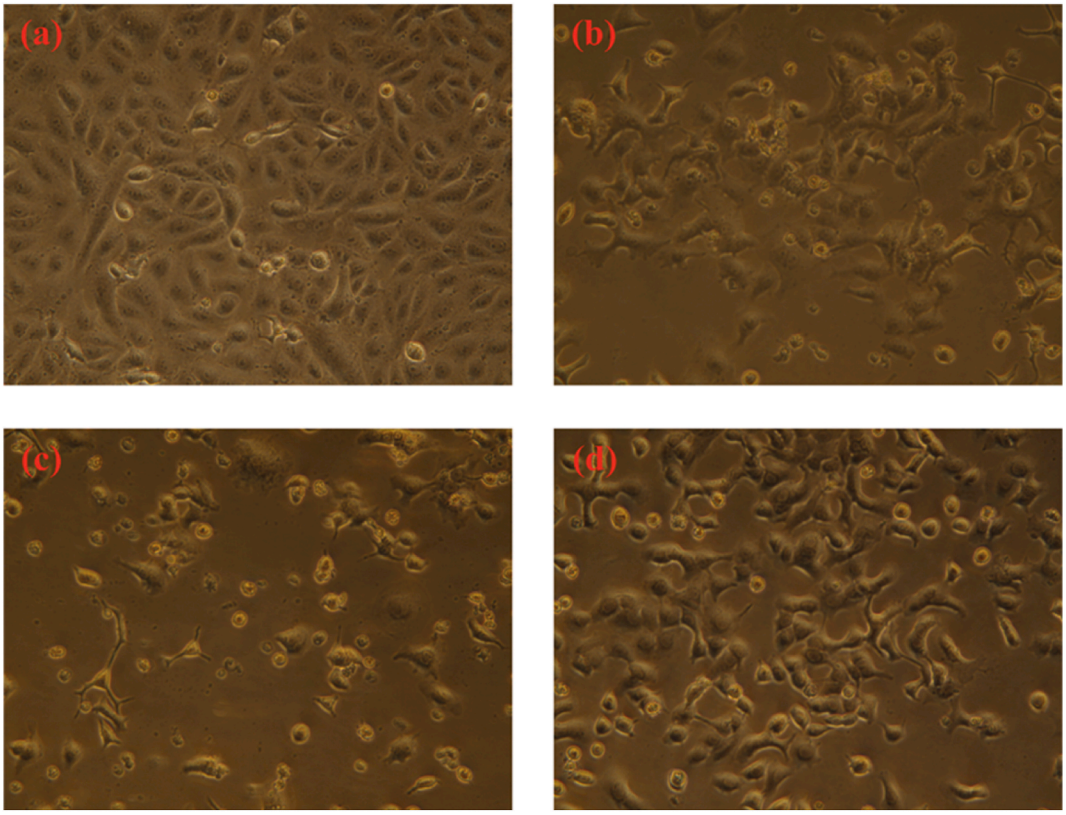


**Fig. 9.** Images of cancer cells matrix captured with an inverted microscope for control (a), 5 μg/mL (b), 10 μg/mL (c), and 20 μg/mL (d).

analysis, Data curation. **Mohammad Abdul Alim:** Visualization. **Md. Chanmiya Sheikh:** Methodology, Investigation, Formal analysis. **Subrata Paul:** Visualization, Data curation.

## Declaration of competing interest

The authors declare that they have no known competing financial interests or personal relationships that could have appeared to influence the work reported in this paper.

## Acknowledgements

The second author, Dr. Tarun Kumar Pal, acknowledges the research project of Rajshahi University of Engineering & Technology (DRE/7/RUET/574/2022-23; Date: 29/06/2022) for providing funds. The second author also acknowledges J. N. Cheerlin Mishma, Department of Physics, Women's Christian College, Nagercoil-629001, Tamil Nadu, India, for the analysis of LOL/ELF and Fukui function and her kind cooperation.

## References

[1] S. Mondal, S.M. Mandal, T.K. Mondal, C. Sinha, Structural characterization of new Schiff bases of sulfamethoxazole and sulfathiazole, their antibacterial activity and docking computation with DHPS protein structure, Spectrochim. Acta Part A Mol. Biomol. Spectrosc. 150 (2015) 268–279, https://doi.org/10.1016/j.saa.2015.05.049.

[2] A. Al Mahmud, T.K. Pal, M. Monirul Islam, M. Masuqul Haque, M. Al-Amin-Al-Azadul Islam, M. Chanmiya Sheikh, R. Miyatake, S. Paul, Experimental and theoretical insights into structural features of methyl (E)-3-(3,4,5-trimethoxybenzylidene)dithiocarbazate with molecular docking and ADMET studies, J. Mol. Struct. 1287 (2023) 135654, https://doi.org/10.1016/j.molstruc.2023.135654.

[3] E. Raczuk, B. Dmochowska, J. Samaszko-Fiertek, J. Madaj, Different Schiff bases—structure, importance and classification, Molecules 27 (2022), https://doi.org/10.3390/molecules27030787.

[4] S. Mondal, S.M. Mandal, T.K. Mondal, C. Sinha, Spectroscopic characterization, antimicrobial activity, DFT computation and docking studies of sulfonamide Schiff bases, J. Mol. Struct. 1127 (2017) 557–567, https://doi.org/10.1016/j.molstruc.2016.08.011.

[5] G. Thilagavathi, A. Kanagavalli, R. Jayachitra, M. Padmavathy, N. Elangovan, R. Thomas, Synthesis, structural, computational, electronic spectra, wave function properties and molecular docking studies of (Z)-4-(((5-methylfuran-2-yl)methylene)amino)-N-(thiazol-2-yl)benzenesulfonamide, J. Indian Chem. Soc. 99 (2022) 100786, https://doi.org/10.1016/j.jics.2022.100786.

[6] Shehnaz, W.A. Siddiqui, M.A. Raza, A. Ashraf, M. Ashfaq, M.N. Tahir, S. Niaz, Structure elucidation {single X-ray crystal diffraction studies, Hirshfeld surface analysis, DFT} and antibacterial studies of sulfonamide functionalized Schiff base copper (II) and zinc (II) complexes, J. Mol. Struct. 1295 (2024) 136603, https://doi.org/10.1016/j.molstruc.2023.136603.

[7] D.M. Gil, F.F. Salomón, G.A. Echeverría, O.E. Piro, H. Pérez, A. Ben Altabef, A detailed exploration of intermolecular interactions in 4-(4-dimethylaminobenzylideneamino)-N-(5-methyl-3-isoxazolyl)benzenesulfonamide and related Schiff bases: crystal structure, spectral studies, DFT methods, Pixel energies and Hirshfeld surface analy, Spectrochim. Acta Part A Mol. Biomol. Spectrosc. 185 (2017) 286–297, https://doi.org/10.1016/j.saa.2017.05.066.

[8] S. Paul, M.A. Alam, T.K. Pal, M.N. Uddin, M.M. Islam, M.C. Sheikh, Quantum computational, spectroscopic investigation, molecular docking, and in vitro pharmacological studies of sulfonamide Schiff base, J. Mol. Struct. 1262 (2022) 133084, https://doi.org/10.1016/j.molstruc.2022.133084.

[9] M. Nur Amin Bitu, Anti-pathogenic activity of Cu(II) complexes incorporating Schiff bases: a short review, Am. J. Heterocycl. Chem. 5 (2019) 11, https://doi.org/10.11648/j.ajhc.20190501.14.

[10] A. Frei, A.D. Verderosa, A.G. Elliott, J. Zuegg, M.A.T. Blaskovich, Metals to combat antimicrobial resistance, Nat. Rev. Chem 7 (2023) 202–224, https://doi.org/10.1038/s41570-023-00463-4.

[11] J.B.N. Moreira, M. Wohlwend, U. Wisløff, Molecular insights, Nat. Metab. 2 (2020) 829–839, https://doi.org/10.1038/s42255-020-0262-1.

[12] R. Jayachitra, M. Padmavathy, A. Kanagavalli, G. Thilagavathi, N. Elangovan, S. Sowrirajan, R. Thomas, Synthesis, computational, experimental antimicrobial activities and theoretical molecular docking studies of (E)-4-((4-hydroxy-3-methoxy-5-nitrobenzylidene) amino)-N-(thiazole-2-yl) benzenesulfonamide, J. Indian Chem. Soc. 100 (2023) 100824, https://doi.org/10.1016/j.jics.2022.100824.

[13] S. Gurusamy, K. Krishnaveni, M. Sankarganesh, V. Sathish, P. Thanasekaran, A. Mathavan, Multiple target detection and binding properties of naphthalene-derived Schiff-base chemosensor, J. Mol. Liq. 325 (2021) 115190, https://doi.org/10.1016/j.molliq.2020.115190.

[14] A.S. Hassan, T.S. Hafez, S.A.M. Osman, M.M. Ali, Synthesis and in vitro cytotoxic activity of novel pyrazolo[1,5-a]pyrimidines and related Schiff bases, Turk. J. Chem. 39 (2015) 1102–1113, https://doi.org/10.3906/kim-1504-12.

[15] A.S. Hassan, A.A. Askar, E.S. Nossier, A.M. Naglah, G.O. Moustafa, M.A. Al-Omar, From 5-Aminopyrazoles, Molecules 24 (2019) 1–12.

[16] M.M. Alnoman, S. Parveen, R.B. Alnoman, A. Khan, M.M. Khaleil, M. Jaremko, I. Al-Younis, A.-H. Emwas, New Co(II) Schiff base complexes of 3-ethoxy-4-hydroxybenzaldehyde and chlorophenyl ethylamine derivatives as potent antimicrobial agents: design, synthesis, molecular docking, DFT calculations, and in silico ADME profiles, J. Mol. Struct. 1307 (2024) 138021, https://doi.org/10.1016/j.molstruc.2024.138021.

[17] S.A. Hassan, D.M. Aziz, M.N. Abdullah, A.R. Bhat, R.S. Dongre, S. Ahmed, A. Kalilur Rahiman, T. Ben Hadda, M. Berredjem, J. Jamalis, Design and synthesis of oxazepine derivatives from sulfonamide Schiff bases as antimicrobial and antioxidant agents with low cytotoxicity and hemolytic prospective, J. Mol. Struct. 1292 (2023) 136121, https://doi.org/10.1016/j.molstruc.2023.136121.

[18] A. Bouzaheur, A. Bouchoucha, K. Si Larbi, S. Zaater, Experimental and DFT studies of a novel Schiff base sulfonamide derivative ligand and its palladium (II) and platinum (IV) complexes: antimicrobial activity, cytotoxicity, and molecular docking study, J. Mol. Struct. 1261 (2022) 132811, https://doi.org/10.1016/j.molstruc.2022.132811.

[19] A. Garg, A. Vijeata, G. Ram Chaudhary, A. Bhalla, S. Chaudhary, Unveiling the antimicrobial potency and binding interaction between sulfonamide substituted Schiff's bases and BSA protein: an integrated experimental and theoretical approach, J. Mol. Liq. 401 (2024) 124710, https://doi.org/10.1016/j.molliq.2024.124710.

[20] A.A. Abdulridha, M.A. AlboHayAllah, S.Q. Makki, Y. Sert, H.E. Salman, A.A. Balakit, Corrosion inhibition of carbon steel in 1 M H2SO4 using new Azo Schiff compound: electrochemical, gravimetric, adsorption, surface and DFT studies, J. Mol. Liq. 315 (2020) 113690, https://doi.org/10.1016/j.molliq.2020.113690.

[21] M. J. Frisch, G.W. Trucks, H.B. Schlegel, G.E. Scuseria, M.A. Robb, J.R. Cheeseman, G. Scalmani, V. Barone, B. Mennucci, G.A. Petersson, H. Nakatsuji, M. Caricato, X. Li, H.P. Hratchian, A.F. Izmaylov, J. Bloino, G. Zheng, J.L. Sonnenberg, M. Hada, M. Ehara, K. Toyota, R. Fukuda, J. Hasegawa, M. Ishida, T. Nakajima, Y. Honda, O. Kitao, H. Nakai, T. Vreven, Jr.J.A. Montgomery, J.E. Peralta, F. M. Ogliaro, J. Bearpark, J. Heyd, E. Brothers, K.N. Kudin, V.N. Staroverov, R. Kobayashi, J. Normand, K. Raghavachari, A. Rendell, J.C. Burant, S.S. Iyengar, J. Tomasi, M. Cossi, N. Rega, J.M. Millam, M. Klene, O.Yazyev, A. J. Austin, R. Cammi, C. Pomelli, J.W.Ochterski, R.L.Martin, K. Morokuma, V. G. Zakrzewski, G.A.P.; Salvador, J.J. Dannenberg, S. Dapprich, A.D. Daniels, Ö. Farkas, J.B. Foresman, J.V. Ortiz, J. Cioslowski, D.J. Fox, Gaussian, Inc., CT Wallingford, 2009.

[22] T. Lu, F. Chen, Multiwfn: a multifunctional wavefunction analyzer, J. Comput. Chem. 33 (2012) 580–592, https://doi.org/10.1002/jcc.22885.

[23] Y. Yamada, S. Gohda, K. Abe, T. Togo, N. Shimano, T. Sasaki, H. Tanaka, H. Ono, T. Ohba, S. Kubo, T. Ohkubo, S. Sato, Carbon materials with controlled edge structures, Carbon N. Y. 122 (2017) 694–701, https://doi.org/10.1016/j.carbon.2017.07.012.

[24] Roy D. Dennington, Todd A. Keith and John M. Millam, Semichem, Inc., 2016.

[25] J.H. Solanki, S.I. Marjadi, Synthesis and antimicrobial study of some novel Schiff bases and formazans, Der Pharma Chem. 8 (2016) 80–85.

[26] S. Alyar, T. Şen, Ü.Ö. Özmen, H. Alyar, Ş. Adem, C. Şen, Synthesis, spectroscopic characterizations, enzyme inhibition, molecular docking study and DFT calculations of new Schiff bases of sulfa drugs, J. Mol. Struct. 1185 (2019) 416–424, https://doi.org/10.1016/j.molstruc.2019.03.002.

[27] M. Tahriri, M. Yousefi, K. Mehrani, M. Tabatabaee, M.D. Ashkezari, Synthesis, characterization and antimicrobial activity of two novel sulfonamide Schiff base compounds, Pharm. Chem. J. 51 (2017) 425–428, https://doi.org/10.1007/s11094-017-1626-z.

[28] M.P. Andersson, P. Uvdal, (1 - 1, 2 (2005) 2937–2941.

[29] M. Riaz, F. Jan, A. Khan, A. Ullah, H. Haq, A.F. AlAsmari, M. Alharbi, F. Alasmari, MominKhan, Unraveling the molecular structure, spectroscopic properties, and antioxidant activities of new 2,4-dinitrophenylhydrazone derivatives through a comprehensive investigation, Arab. J. Chem. 16 (2023) 105259, https://doi.org/10.1016/j.arabjc.2023.105259.

[30] R. Farooq, Z. Batool, M. Khalid, M.U. Khan, A.A. Carmo Braga, A.H. Ragab, S.R. Al-Mhyawi, G. Muhammad, Z. Shafiq, Synthesis, nonlinear optical analysis and DFT studies of D-π-D and A-π-A configured Schiff bases derived from bis-phenylenediamine, RSC Adv. 12 (2022) 32185–32196, https://doi.org/10.1039/d2ra05844h.

[31] K. Vibha, N.C. Prachalith, R. Annoji Reddy, M.N. Ravikantha, J. Thipperudrappa, Computational studies on sulfonamide drug molecules by density functional theory, Chem. Phys. Impact 6 (2023) 100147, https://doi.org/10.1016/j.chphi.2022.100147.

[32] B.P. Sharma, J. Adhikari Subin, B.P. Marasini, R. Adhikari, S.K. Pandey, M.L. Sharma, Triazole based Schiff bases and their oxovanadium(IV) complexes: synthesis, characterization, antibacterial assay, and computational assessments, Heliyon 9 (2023) e15239, https://doi.org/10.1016/j.heliyon.2023.e15239.

[33] K. Benbouguerra, N. Chafai, S. Chafaa, Y.I. Touahria, H. Tlidjane, New α-Hydrazinophosphonic acid: synthesis, characterization, DFT study and in silico prediction of its potential inhibition of SARS-CoV-2 main protease, J. Mol. Struct. 1239 (2021) 130480, https://doi.org/10.1016/j.molstruc.2021.130480.

[34] D.M. Mamand, Electronic structure , Optoelectronic properties, in: FTIR , CNMR and HNMR Investigation on 4- (( 2-hydroxy-3- Benzene Sulfonamide Molecules at Different Concentrations in DMSO Solvent, 2022, pp. 1–2.

[35] A.I. Aljameel, DFT study of 4-acetamido-N-(3-amino-1,2,4-triazol-1-yl) benzene sulfonamide and its potential application as copper corrosion inhibitor, Int. J. Electrochem. Sci. 17 (2022) 220524, https://doi.org/10.20964/2022.05.39.

[36] N. Nehra, R.K. Tittal, V.D. Ghule, 1,2,3-Triazoles of 8-hydroxyquinoline and HBT: synthesis and studies (DNA binding, antimicrobial, molecular docking, ADME, and DFT), ACS Omega 6 (2021) 27089–27100, https://doi.org/10.1021/acsomega.1c03668.

[37] J.S. Singh, M.S. Khan, S. Uddin, A DFT study of vibrational spectra of 5-chlorouracil with molecular structure, HOMO–LUMO, MEPs/ESPs and thermodynamic properties, Polym. Bull. 80 (2023) 3055–3083, https://doi.org/10.1007/s00289-022-04181-7.

[38] D.D. Li, M.L. Greenfield, Chemical compositions of improved model asphalt systems for molecular simulations, Fuel 115 (2014) 347–356, https://doi.org/10.1016/j.fuel.2013.07.012.

[39] K. Merdja, C.K. Bendeddouche, M. Drissi, F.C. Kaouche, N. Medjahed, J.M. Padrón, M. Debdab, M. Rahmouni, E.H. Belarbi, pt, (2023) 1–13. https://doi.org/10.22146/ijc.87476.

[40] N. Elangovan, S. Sowrirajan, K.P. Manoj, A.M. Kumar, Synthesis, structural investigation, computational study, antimicrobial activity and molecular docking studies of novel synthesized (E)-4-((pyridine-4-ylmethylene)amino)-N-(pyrimidin-2-yl)benzenesulfonamide from pyridine-4-carboxaldehyde and sulfadiazine, J. Mol. Struct. 1241 (2021) 130544, https://doi.org/10.1016/j.molstruc.2021.130544.

[41] C. Sivakumar, B. Revathi, V. Balachandran, B. Narayana, V.V. Salian, N. Shanmugapriya, K. Vanasundari, Molecular structure, spectroscopic, quantum chemical, topological, molecular docking and antimicrobial activity of 3-(4-Chlorophenyl)-5-[4-propan-2-yl) phenyl-4, 5-dihydro-1H-pyrazol-1-yl] (pyridin-4-yl) methanone, J. Mol. Struct. 1224 (2021) 129286, https://doi.org/10.1016/j.molstruc.2020.129286.
[42] Y. Oueslati, S. Kansız, A. Valkonen, T. Sahbani, N. Dege, W. Smirani, Synthesis, crystal structure, DFT calculations, Hirshfeld surface, vibrational and optical properties of a novel hybrid non-centrosymmetric material (C10H15N2)2H2P2O7, J. Mol. Struct. 1196 (2019) 499–507, https://doi.org/10.1016/j.molstruc.2019.06.110.
[43] S. Kanchana, T. Kaviya, P. Rajkumar, M.D. Kumar, N. Elangovan, S. Sowrirajan, Computational investigation of solvent interaction (TD-DFT, MEP, HOMO-LUMO), wavefunction studies and molecular docking studies of 3-(1-(3-(5-((1-methylpiperidin-4-yl)methoxy)pyrimidin-2-yl)benzyl)-6-oxo-1,6-dihydropyridazin-3-yl)benzonitrile, Chem. Phys. Impact 7 (2023) 100263, https://doi.org/10.1016/j.chphi.2023.100263.
[44] A.H. Shamina, V. Ganesan, V.B. Jothy, A. Manikandan, S. Muthu, S. Javed, Quantum chemical computations on molecular composition, spectroscopic properties, topology exploration, NLO, ligand protein interactions and pharmacokinetic evaluation of 8-hydroxyquinolium 3-nitrobenzoate, Chem. Phys. Impact 8 (2024) 100394, https://doi.org/10.1016/j.chphi.2023.100394.
[45] T.K. Pal, M.A. Mumit, J. Hossen, S. Paul, M.A. Alam, M.A.A.A.A. Islam, M.C. Sheikh, Computational and experimental insight into antituberculosis agent, (E)-Benzyl-2-(4-Hydroxy-2-Methoxybenzylidene) hydrazinecarbodithioate: adme analysis, Heliyon 7 (2021) e08209, https://doi.org/10.1016/j.heliyon.2021.e08209.
[46] S.C. Parakkal, R. Datta, S. Muthu, A. Irfan, A. Jeelani, Computational investigation into structural, topological, electronic properties, and biological evaluation of spiro[1H-indole-3,2′-3H-1,3-benzothiazole]-2-one, J. Mol. Liq. 359 (2022) 119234, https://doi.org/10.1016/j.molliq.2022.119234.
[47] G. Kanimozhi, S. Tamilselvan, K.M. Potla, J.N. Cheerlin Mishma, F. Akman, M. Vimalan, N.S. Alharbi, G. Abbas, S. Muthu, Solvents performance, experimental spectral energies interactions, excitations energies, topological and electrophilic molecular interaction studies on 4?-(bromomethyl)-[1,1?-biphenyl]-2-carbonitrile- antiphobic disorder agent, J. Mol. Liq. 391 (2023) 123368, https://doi.org/10.1016/j.molliq.2023.123368.
[48] A.H. Shamina, V.B. Jothy, Spectroscopic characterization, DFT study, topological, molecular docking and pharmacological analysis of Iminodiacetic acid Hydrochloride, J. Mol. Liq. 387 (2023) 122599, https://doi.org/10.1016/j.molliq.2023.122599.
[49] M. Vimala, S. Stella Mary, R. Ramalakshmi, S. Muthu, R. Niranjana Devi, A. Irfan, Quantum computational studies on optimization, donor-acceptor analysis and solvent effect on reactive sites, global descriptors, non-linear optical parameters of Methyl N-Boc-piperidine-3-carboxylate, J. Mol. Liq. 343 (2021) 117608, https://doi.org/10.1016/j.molliq.2021.117608.
[50] J. Geethapriya, A. Shanthidevi, M. Arivazhagan, N. Elangovan, R. Thomas, Synthesis, structural, DFT, quantum chemical modeling and molecular docking studies of (E)-4-(((5-methylfuran-2-yl)methylene)amino) benzenesulfonamide from 5-methyl-2-furaldehyde and sulfanilamide, J. Indian Chem. Soc. 99 (2022) 100418, https://doi.org/10.1016/j.jics.2022.100418.
[51] Y.S. Mary, Y.S. Mary, A.S. Rad, R. Yadav, I. Celik, S. Sarala, Theoretical investigation on the reactive and interaction properties of sorafenib – DFT, AIM, spectroscopic and Hirshfeld analysis, docking and dynamics simulation, J. Mol. Liq. 330 (2021) 115652, https://doi.org/10.1016/j.molliq.2021.115652.
[52] J. Geethapriya, A. Shanthidevi, M. Arivazhagan, N. Elangovan, R. Thomas, Synthesis, structural, DFT, quantum chemical modeling and molecular docking studies of (E)-4-(((5-methylfuran-2-yl)methylene)amino) benzenesulfonamide from 5-methyl-2-furaldehyde and sulfanilamide, J. Indian Chem. Soc. 99 (2022) 100418, https://doi.org/10.1016/j.jics.2022.100418.
[53] V. Rajmohan, S. Deepa, S. Asha, S.V. Priya, A. Sagaama, M. Raja, Synthesis, solvation effects, spectroscopic, chemical reactivity, topological analysis and biological evaluation of 4-chloro-N-(2, 6-dichlorobenzylidene) benzohydrazide, J. Mol. Liq. 390 (2023) 122955, https://doi.org/10.1016/j.molliq.2023.122955.
[54] V.S. Jeba Reeda, V. Bena Jothy, Vibrational spectroscopic, quantum computational (DFT), reactivity (ELF, LOL and Fukui), molecular docking studies and molecular dynamic simulation on (6-methoxy-2-oxo-2H-chromen-4-yl) methyl morpholine-4-carbodithioate, J. Mol. Liq. 371 (2023) 121147, https://doi.org/10.1016/j.molliq.2022.121147.
[55] A.D. Isravel, J.K. Jeyaraj, S. Thangasamy, W.J. John, D.F.T. Nbo, HOMO-LUMO, NCI, stability, Fukui function and hole – electron analyses of tolcapone, Comput. Theor. Chem. 1202 (2021) 113296, https://doi.org/10.1016/j.comptc.2021.113296.
[56] V. Pilepi, S. Urši, Nucleophilic reactivity of the nitroso group. Fukui function DFT calculations for nitrosobenzene and 2-methyl-2-nitrosopropane, J. Mol. Struct. THEOCHEM. 538 (2001) 41–49, https://doi.org/10.1016/S0166-1280(00)00642-4.
[57] A. Saral, P. Sudha, S. Muthu, S. Sevvanthi, A. Irfan, Molecular structure spectroscopic Elucidation, IEFPCM solvation (UV–Vis, MEP, FMO, NBO, NLO), molecular docking and biological assessment studies of lepidine (4-Methylquinoline), J. Mol. Liq. 345 (2022) 118249, https://doi.org/10.1016/j.molliq.2021.118249.
[58] C.U. Maheswari, QM, Fukui function, molecular docking, molecular dynamics investigation on Human Estrogen Receptor (HER) with Clioquinol, Chem. Phys. Impact 8 (2024), https://doi.org/10.1016/j.chphi.2024.100570.
[59] S. Şahin, 4,5-difluoro-2-((m-tolylimino)methyl)phenol: investigations on a synthesized Schiff base with in silico medicinal approaches and DFT studies, J. Mol. Struct. 1306 (2024) 1–13, https://doi.org/10.1016/j.molstruc.2024.137882.
[60] V.S. Jeba Reeda, V. Bena Jothy, Vibrational spectroscopic, quantum computational (DFT), reactivity (ELF, LOL and Fukui), molecular docking studies and molecular dynamic simulation on (6-methoxy-2-oxo-2H-chromen-4-yl) methyl morpholine-4-carbodithioate, J. Mol. Liq. 371 (2023) 121147, https://doi.org/10.1016/j.molliq.2022.121147.
[61] Y.S. Mary, H.T. Varghese, C.Y. Panicker, T. Thiemann, A.A. Al-Saadi, S.A. Popoola, C. Van Alsenoy, Y. Al Jasem, Molecular conformational analysis, vibrational spectra, NBO, NLO, HOMO-LUMO and molecular docking studies of ethyl 3-(E)-(anthracen-9-yl)prop-2-enoate based on density functional theory calculations, Spectrochim. Acta Part A Mol. Biomol. Spectrosc. 150 (2015) 533–542, https://doi.org/10.1016/j.saa.2015.05.092.
[62] S. Chigurupati, V.R. Palanimuthu, S. Kanagaraj, S. Sundaravadivelu, V.R. Varadharajula, Green synthesis and in silico characterization of 4-Hydroxy-3-methoxybenzaldehyde Schiff bases for insulysin inhibition – a potential lead for type 2 diabetes mellitus, J. Appl. Pharmaceut. Sci. 11 (2021) 63–71, https://doi.org/10.7324/JAPS.2021.110706.
[63] P. Ramesh, M. Lydia Caroline, S. Muthu, B. Narayana, M. Raja, S. Aayisha, Spectroscopic and DFT studies, structural determination, chemical properties and molecular docking of 1-(3-bromo-2-thienyl)-3-[4-(dimethylamino)-phenyl]prop-2-en-1-one, J. Mol. Struct. 1200 (2020), https://doi.org/10.1016/j.molstruc.2019.127123.
[64] B. Amul, S. Muthu, M. Raja, S. Sevvanthi, Molecular structure, spectroscopic (FT-IR, FT-Raman, NMR, UV-VIS), chemical reactivity and biological examinations of Ketorolac, J. Mol. Struct. 1210 (2020) 128040, https://doi.org/10.1016/j.molstruc.2020.128040.
[65] Y. Sert, M.R. Albayati, F. Şen, N. Dege, The DFT and in-silico analysis of 2,2′-((1e,1′e)-((3,3′-dimethyl-[1,1′-biphenyl]−4,4′ diyl)bis(azanylylidene))bis(methanylylidene))diphenol molecule, Colloids Surfaces A Physicochem. Eng. Asp. 687 (2024), https://doi.org/10.1016/j.colsurfa.2024.133444.
[66] M. Gümüş, Ş.N. Babacan, Y. Demir, Y. Sert, İ. Koca, İ. Gülçin, Discovery of sulfadrug–pyrrole conjugates as carbonic anhydrase and acetylcholinesterase inhibitors, Arch. Pharm. (Weinheim) (2022) 355, https://doi.org/10.1002/ardp.202100242.
[67] A. Allouche, Software news and updates gabedit — a graphical user interface for computational chemistry softwares, J. Comput. Chem. 32 (2012) 174–182, https://doi.org/10.1002/jcc.
[68] E. Havránková, N. Čalkovská, T. Padrtová, J. Csöllei, R. Opatřilová, P. Pazdera, Antioxidative activity of 1,3,5-triazine analogues incorporating aminobenzene sulfonamide, aminoalcohol/phenol, piperazine, chalcone, or stilbene motifs, Molecules 25 (2020) 7–9, https://doi.org/10.3390/molecules25081787.
[69] N.L. Parinandi, N. Maulik, M. Thirunavukkarasu, D.W. McFadden, Antioxidants in longevity and medicine 2014, Oxid. Med. Cell. Longev. 2015 (2015), https://doi.org/10.1155/2015/739417.
[70] T. Persson, B.O. Popescu, A. Cedazo-Minguez, Oxidative stress in alzheimer's disease: why did antioxidant therapy fail? Oxid. Med. Cell. Longev. 2014 (2014) https://doi.org/10.1155/2014/427318.
[71] P. Gonzalez, K. Pota, L.S. Turan, V.C.P. Da Costa, G. Akkaraju, K.N. Green, Synthesis, characterization, and activity of a triazine bridged antioxidant small molecule, ACS Chem. Neurosci. 8 (2017) 2414–2423, https://doi.org/10.1021/acschemneuro.7b00184.
[72] S. Toda, Polyphenol content and antioxidant effects in herb teas, Chin. Med. 2 (2011) 29–31, https://doi.org/10.4236/cm.2011.21005.

[73] C. López-Alarcón, A. Denicola, Evaluating the antioxidant capacity of natural products: a review on chemical and cellular-based assays, Anal. Chim. Acta 763 (2013) 1–10, https://doi.org/10.1016/j.aca.2012.11.051.
[74] A.M. Pisoschi, A. Pop, The role of antioxidants in the chemistry of oxidative stress: a review, Eur. J. Med. Chem. 97 (2015) 55–74, https://doi.org/10.1016/j.ejmech.2015.04.040.
[75] K. Neha, M.R. Haider, A. Pathak, M.S. Yar, Medicinal prospects of antioxidants: a review, Eur. J. Med. Chem. 178 (2019) 687–704, https://doi.org/10.1016/j.ejmech.2019.06.010.
[76] N. Lolak, M. Tuneğ, A. Doğan, M. Boğa, S. Akocak, Synthesis and biological evaluation of 1,3,5-triazine-substituted ureido benzenesulfonamides as antioxidant, acetylcholinesterase and butyrylcholinesterase inhibitors, Bioorganic Med. Chem. Reports 3 (2020) 22–31, https://doi.org/10.25135/acg.bmcr.22.20.07.1706.
[77] M.J. Mphahlele, S. Gildenhuys, S.J. Zamisa, Synthesis, structure and evaluation of the N-(2-Acetyl-4-(styryl)phenyl)-4-benzenesulfonamide derivatives for anticholinesterase and antioxidant activities, Crystals (2021) 11, https://doi.org/10.3390/cryst11040341.